

Application of noble gas tracers to identify the retention mechanisms of CO₂ migrated from a deep reservoir into shallow groundwater

YeoJin Ju^a, Stuart M.V. Gilfillan^b, Seong-Sun Lee^a, Dugin Kaown^a, Doshik Hahm^c, Sanghoon Lee^a, In-Woo Park^a, Seung-Wook Ha^a, Keyhong Park^d, Hyun-Kwon Do^e, Seong-Taek Yun^e, Kang-Kun Lee^{a,*}

^a School of Earth and Environmental Sciences, Seoul National University, 1 Gwanak-ro, Gwanak-gu, Seoul, 08826, South Korea

^b School of GeoSciences, The University of Edinburgh, Grant Institute, James Hutton Road, Edinburgh, EH9 3FE, UK

^c Department of Oceanography, Pusan National University, Busan, South Korea

^d Korea Polar Research Institute, Incheon, South Korea

^e Department of Earth and Environmental Sciences, Korea University, Seoul, 02841, South Korea

ARTICLE INFO

Keywords:

CCS
Monitoring
CO₂ leakage
Noble gas tracing
Artificial tracer
Geochemical Monitoring

ABSTRACT

Carbon Capture and Storage (CCS) is a valuable climate-mitigation technology, which offers the potential to cost-effectively reduce the emissions associated with the burning of fossil fuels. However, there is a potential risk of a small portion of the stored CO₂ unintentionally migrating from a storage site to a shallow groundwater aquifer which is the final retaining zone for any migrated CO₂ before it escapes to the atmosphere. Hence, it is imperative to identify the physical retention mechanisms of CO₂ within a shallow aquifer. In this study 1.70 × 10² kg of CO₂ and noble gas tracers (He, Ar and Kr) were continuously injected into a groundwater aquifer over 28 days with the aim of identifying the mechanisms and amount of CO₂ retention. Among the tracers, Kr was found to be the earliest indicator of CO₂ migration. The other tracers – He and Ar – arrived later and exhibited diluted signals. The diluted signals were attributed to degassing of the plume mass (1.6 % of CO₂) during the early stages of CO₂ migration. Diffusion accelerated the dilution of the lighter elements at the plume boundaries. Consequently, the clear relation of the noble gases with the CO₂ proved that degassing and mixing primarily control the mass retention of CO₂ in shallow groundwater, and the relative importance of these processes varies along the evolving path of migrating CO₂.

1. Introduction

Carbon Capture and Storage (CCS) is a climate change mitigation technology that comprises the capture of CO₂ from an industrial point source, such as a power plant or refinery, transport of the captured CO₂ to a storage site followed by the injection of the captured CO₂ into deep geological strata for permanent disposal (IPCC, 2005). However, there is a potential risk that a small portion of the mobile CO₂ in a storage site could accidentally migrate out of the subsurface reservoir and inadvertently reach shallower levels of the subsurface (Alcalde et al., 2018). This CO₂ could potentially migrate through geological conduits such as permeable faults and/or abandoned wells resulting in the deterioration of fresh water resources above the CO₂ reservoir (Harvey et al., 2012; IEAGHG, 2011; Lemieux, 2011; Lions et al., 2014) and leakage of a

small portion of the CO₂ into the atmosphere (Ide et al., 2006; IPCC, 2005). Recently, the Weyburn-Midale (Canada) CO₂ monitoring and storage project faced allegations that leakage of CO₂ injected into the Weyburn-Midale oil field for Enhanced Oil Recovery (EOR) and storage was causing a deterioration of the groundwater quality on a farm located above the field (Beaubien et al., 2013; Gilfillan et al., 2017).

A variety of geochemical tools have been used to verify CO₂ storage security and track the fate of CO₂ injected for storage. These include CO₂ soil gas and groundwater concentrations, stable C and O isotopes within the CO₂, on-site monitoring parameters (pH, alkalinity, ORP, EC, temperature and DO), inert gas tracers, major and trace ions and radiocarbon (¹⁴C) (Flude et al., 2016; Lee et al., 2016). Soil gas and dissolved CO₂ concentrations in groundwater can provide a direct tracer of CO₂ migration, allowing discrimination of different CO₂

* Corresponding author.

E-mail addresses: jinee18@snu.ac.kr (Y. Ju), stuart.gilfillan@ed.ac.uk (S.M.V. Gilfillan), soon3311@snu.ac.kr (S.-S. Lee), dugin1@snu.ac.kr (D. Kaown), hahm@pusan.ac.kr (D. Hahm), lshlsh2311@snu.ac.kr (S. Lee), inwoo0415@snu.ac.kr (I.-W. Park), hasabana@snu.ac.kr (S.-W. Ha), keyhongpark@kopri.re.kr (K. Park), iq1pc@korea.ac.kr (H.-K. Do), styun@korea.ac.kr (S.-T. Yun), kklee@snu.ac.kr (K.-K. Lee).

<https://doi.org/10.1016/j.ijggc.2020.103041>

Received 15 October 2019; Received in revised form 27 March 2020; Accepted 28 March 2020

1750-5836/ © 2020 Elsevier Ltd. All rights reserved.

origins and providing a means to establish the mass balance of CO₂ present in the groundwater system (Ballentine et al., 2001; Beaubien et al., 2014; Gilfillan et al., 2011; Lollar et al., 1997; Sathaye et al., 2016). Recent developments in on-site monitoring technologies now allow the continuous measurement of a number of parameters (e.g. alkalinity, T, EC, pH) which can be used to establish the overall distribution and temporal evolution of a small CO₂ plume within a shallow groundwater aquifer (Lee et al., 2016). Noble gases are characterized by their inert behavior, which makes them ideal tracers within a subsurface system. This inertness means that noble gases are conservative tracers and do not partake in the chemical reactions that dilute the CO₂ leakage signals and hence are capable of providing a robust means to distinguish between natural and stored CO₂ (Risk et al., 2015).

Noble gas tracing techniques have been used to track both the fate and migration pathways of injected CO₂ in reservoirs. Within a typical porous CO₂ storage reservoir, CO₂ is retained by a combination of structural, residual and solubility trapping mechanisms (Alcalde et al., 2018; Holland and Gilfillan, 2013; IPCC, 2005). Recent experiments at the CO₂CRC Otway Demonstration site for CO₂ storage in Australia have used Kr and Xe as conservative tracers to determine the degree of residual trapping within a porous saline formation, using a numerical mass balance approach (LaForce et al., 2014). The degree of solubility trapping has also been determined using noble gases, through identification of the degree of partitioning of the noble gases into groundwater present within the reservoir formations (Ballentine et al., 1991; Brennwald et al., 2005; Gilfillan et al., 2008, 2009, 2014; Pinti and Marty, 1995; Zhou et al., 2005).

Noble gas tracers are also suitable for monitoring the vertical migration of the reservoir CO₂, thanks to the compositional difference of natural noble gas tracers between storage reservoir and the near surface environment (Mackintosh and Ballentine, 2012). Gilfillan et al. (2011) applied noble gas tracing tools to constrain the nature of CO₂ leakage into shallow groundwater and surface water bodies. Further work by Gilfillan et al. (2017) used inherent tracers residing in the Weyburn-Midale injection and storage project reservoir to show that CO₂ migration from the deep reservoir into the shallow aquifer system had not occurred. This work found that the noble gas composition in the groundwater samples above the CO₂ injection and storage project did not vary over a typical background level of a shallow aquifer, of Air Saturated Water (ASW) with an excess air component of up to 45 % (Gilfillan et al., 2017). Recent work by Flude et al. (2016) and Flude et al. (2017) evaluated the inherent tracing ability of noble gases focusing on the compositional difference of them between captured CO₂, the subsurface storage reservoir, air and ASW. Differences in the noble gas contents of these samples stemmed from the different CO₂ capturing processes and what controls the composition of noble gas tracer in a stored fluid (e.g. gas stripping of reservoir water and/or interaction with radiogenic components).

The concept of inert tracers was extended to artificial enhancement studies, involving the addition of inert gas tracers such as SF₆ and noble gases to the injected CO₂ in CCS storage. This aimed to provide a much clearer distinction between the injected CO₂ and that naturally present in the subsurface and so improving the monitoring efficiency (Myers et al., 2013; Nimz and Hudson, 2005). For example, noble gases have been previously used as artificial tracers to indicate CO₂ leakage pathways in the vadose zone (Cohen et al., 2013; Rillard et al., 2015) and in the aquifer system (Lu et al., 2012; Nimz and Hudson, 2005; Stalker et al., 2009). In the CO₂-Vadose project, undertaken at a test CO₂ release site in France, the lighter noble gases (He and Ne) were found to have the fastest arrival time in monitoring wells due to their higher diffusion coefficient and low solubility within the soil water compared to the CO₂ and other tracers (Cohen et al., 2013). In contrast, the heavier noble gas tracers (Kr and Xe) exhibited the fastest arrival in the aquifer system due to their solubility in groundwater compared to other noble gases following the artificial injection into a deep reservoir (~2 km) (Stalker et al., 2015). In a recent test, a small amount of CO₂

(16.9 kg) spiked with noble gas was released into a shallow aquifer at Korea CO₂ Storage Environmental Management (K-COSEM) study site, in order to understand the behavior of the leaked plume in the shallow groundwater system. This study identified that the mass distribution of the leaked CO₂ is predominantly controlled by the solubility of the individual noble gases and mixing processes during the limited time of monitoring work (i.e. 4 months) (Ju et al., 2019).

The shallow groundwater is the final zone encountered by migrating CO₂ before it is lost into the vadose zone and atmosphere. Furthermore, this reservoir is directly linked into the human activity, hence, should be protected from a potential leakage of stored CO₂ (Lee et al., 2016). While noble gas tracers have proven useful to monitor leaked CO₂ plume in shallow aquifer systems (Flude et al., 2016, 2017), this has only been demonstrated on a few occasions, for example, in a natural CO₂ production site using inherent noble gases (Gilfillan et al., 2011), in a CO₂ injection test site using artificially enhanced noble gases (Ju et al., 2019) and to rule out CO₂ migration in a shallow aquifer above an actual CO₂ storage reservoir using inherent noble gases (Gilfillan et al., 2017), as described above. In this study, we present the results of applying noble gases to a CO₂ injection test into a near-surface aquifer. This artificial CO₂ migration test aims to mimic a situation where a measurable amount of CO₂ (1.70×10^2 kg) has migrated from a deep CO₂ storage reservoir into a shallow groundwater aquifer. This study focuses on determining the amount of CO₂ retained in the groundwater and the mechanisms controlling the migration of the CO₂ plume using noble gas tracers. A mass balance model was constructed based on the partitioning coefficients of noble gas tracers in a gas-water system, to understand and to quantify the final retention of the injected CO₂ within the shallow aquifer system.

2. Materials and methods

2.1. Site description

The Korea CO₂ Storage Environmental Management (K-COSEM) Research Center has installed a controlled CO₂ release experiment at Eumseong gun (county) of South Korea (Fig. 1). The geology at the field experimental site includes three different subsurface media, firstly consisting of a weathered soil layer composed of medium to coarse grained silty sand (0–30 m below ground surface (bgs)), followed by weathered biotite granite (30–70 m bgs), and finally consolidated biotite granite (starting at 70 m bgs) (Lee et al., 2017; Ju et al., 2018a). The water level was located at the 16.0–18.4 m bgs and the hydraulic conductivity of the aquifer was estimated from pumping tests, ranging from 1.7×10^{-5} cm/s for the consolidated bedrock to 2.0×10^{-4} cm/s for the weathered layer. Prior to the commencement of the experiment, the groundwater was flowing from the northwest toward the southeast following a hydraulic gradient of 0.003 (i.e., the regional flow in Fig. 1a).

At the K-COSEM site, a total of 24 monitoring wells had been installed in the shallow aquifer (i.e. < 15 m below the water table) including the injection well (IW), partially screened (PS), boreholes (BH), borehole screened (BS) and saturated zone monitoring wells (SMWs) (Fig. 1a). Each saturated zone monitoring well (SMW) contained several screened multi-depth monitoring wells for groundwater monitoring at different depths (Fig. 1f). In this CO₂ injection study, the IW and six monitoring wells (PS-04, SMW1 to 4, BS-04, -09 and -10) were employed for the CO₂ injection experiment (Fig. 1b). The wells BS-04 and BS-10 located at both ends of the monitoring range were used to create an induced pressure gradient field by pumping out groundwater at a down-gradient location (BS-10) and successive injection in at an up-gradient location (BS-4) (Fig. 1c). The SMWs are located along the created groundwater flow pathway, while PS-04 was up-gradient relative to the CO₂ injection point. The well BS-09 was intended to capture the preferential movement of the released CO₂ along a high connectivity zone between injection well and BS-09, identified in the work

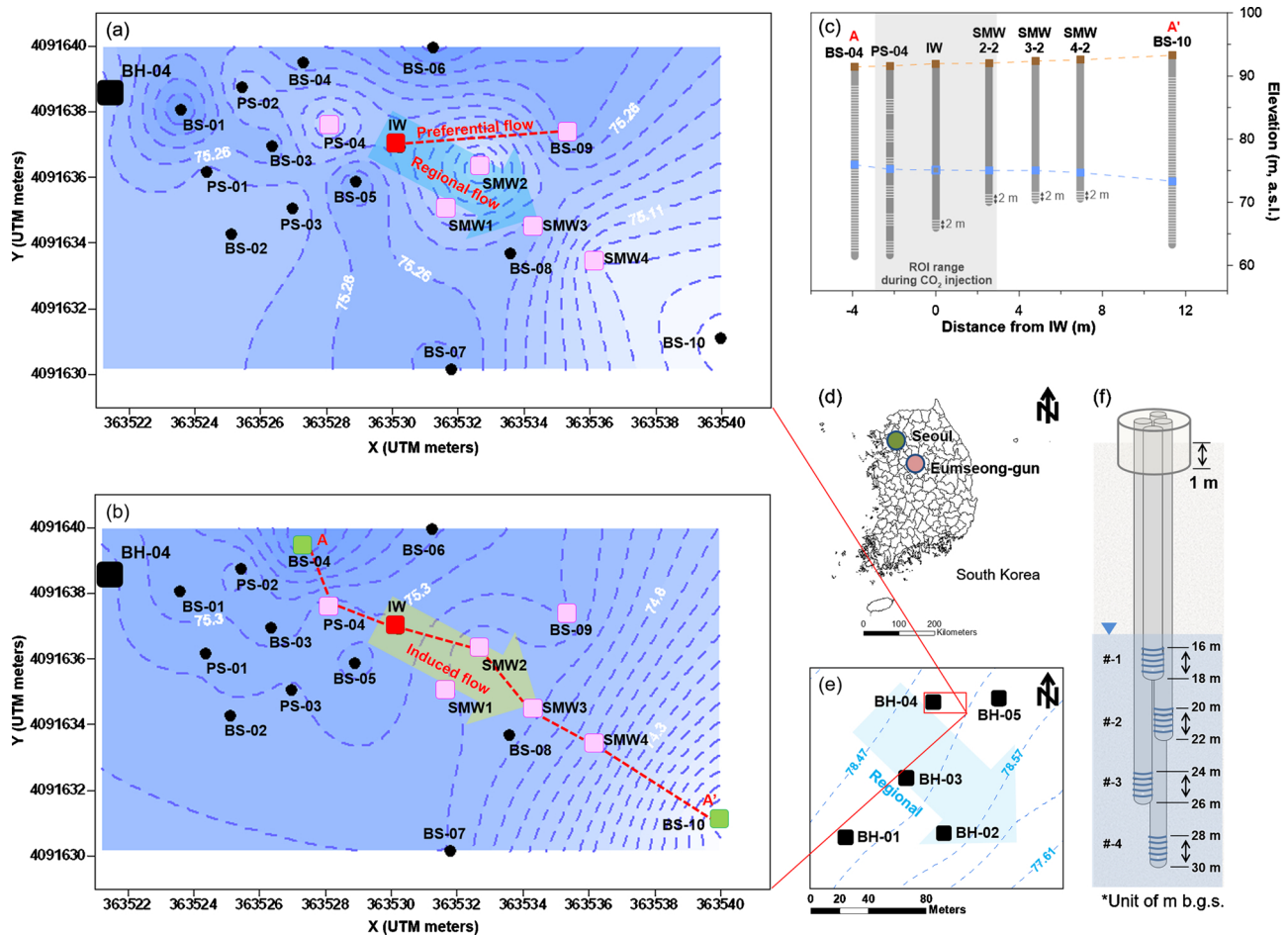


Fig. 1. Maps of the study site. Figures on the left show (a) natural regional groundwater flow (shown as a blue-colored arrow) before enhanced groundwater circulation using the wells BS-04 and BS-10, where a preferential path exists in this field due to local hydrogeological heterogeneity (16 May 2016), (b) induced pressure gradient field (shown as a green-colored arrow) after the pumping out and pumping in using the two wells (see green squares) (4 July 2016). Note that the induced flow was intended to speed up the plume migration along the groundwater flow (i.e., regional flow in [a]). Pink squares represent the wells used for monitoring; a red square represents the injection well (IW). Figures on the right show (c) a cross-section view along the induced pressure gradient (4 July 2016), (d) the location map of the study area, (e) the contours of groundwater levels obtained by kriging using 17 wells surrounding the study site (7 March 2015), and (f) the structure of each saturated zone monitoring well (SMW) containing a bundle of four screened pipes with different lengths.

of Ju et al. (2019). Details on the study site and monitoring network can also be found in previous works (Lee et al., 2017, 2018; Ju et al., 2018b, 2019).

2.2. Artificial injection

2.2.1. Induced pressure gradient field

The CO₂ injection was undertaken in the induced pressure gradient field to reinforce the groundwater flow, therefore, to speed up the CO₂ plume migration (Fig. 2c). The hydraulic pressure gradient was achieved by enhancing groundwater circulation, consisting of water production and reinjection using the BS-04 and BS-10 wells located at both ends of the monitoring network (Fig. 2c). A total of 24.0 m³/d of groundwater was pumped from BS-10 and reinjected into BS-04 (Fig. 2c). A period of 1 month was required to stabilize the pressure gradient (22 May 2017 to 27 June 2017). The pressure gradient was steeper near the injection site and production points (i.e. the BS-04 and BS-10), with the average gradient being 0.18 (Fig. 2c). The circulation was maintained until 17 September 2017.

2.2.2. Injection

To prepare the injection water, the water flux sent to BS-04 (24.0 m³/d) was reduced to 18.5 m³/d and 5.5 m³/d of groundwater was sent into the injection tank (Fig. 2c). 5.0 m³/d of groundwater was

sent into the CO₂ dissolver tank (Fig. 2b) and 0.5 m³/d of tracer-enhanced water was prepared in the other tank (Fig. 2a). The CO₂-infused groundwater was prepared in the 5 m³ tank equipped with the circulation pump, CO₂ dissolver, water sampling port and flow meter (Fig. 2b). Injection was initiated when the CO₂ concentration reached the equilibrium state (termed C₀). To ensure that the equilibrium concentration was maintained, alkalinity, pH, EC, DO, ORP, temperature, salinity, TDS was continuously monitored with real time measurement devices such as YSI (YSI Inc./Xylem Inc., USA), LTC Levellogger Junior (Solinst, Canada) and SH-300-DS (SOHA TECH, Inc., Korea) while circulating water within the tank using a pump (Fig. 2b). These measurements showed that it took approximately 24 h to achieve the equilibrium state. The noble gas infused groundwater was also prepared one day ahead of the injection test. Approximately 0.5 m³/d of groundwater was pumped into the 1 m³ of closed tank equipped with the circulation pump, tracer tank, water sampling port and flow meter (Fig. 2a). The injected tracers were a mixture of He (0.2 vol. %), Ar (99.4 vol. %), and Kr (0.4 vol. %) and were injected through a flow-meter and diffuser (AS-10 3/8) into the 1 m³ dissolver tank. The infused liquids were first injected into the subsurface on 27 June 2017 and continued to be injected for 27 days until 24 July 2017. Samples for initial concentration analyses (i.e. C₀) were collected during the injection event and through the sampling ports (Fig. 2a and b). Injection took place at 4.5–7.5 m below the water table (corresponding to

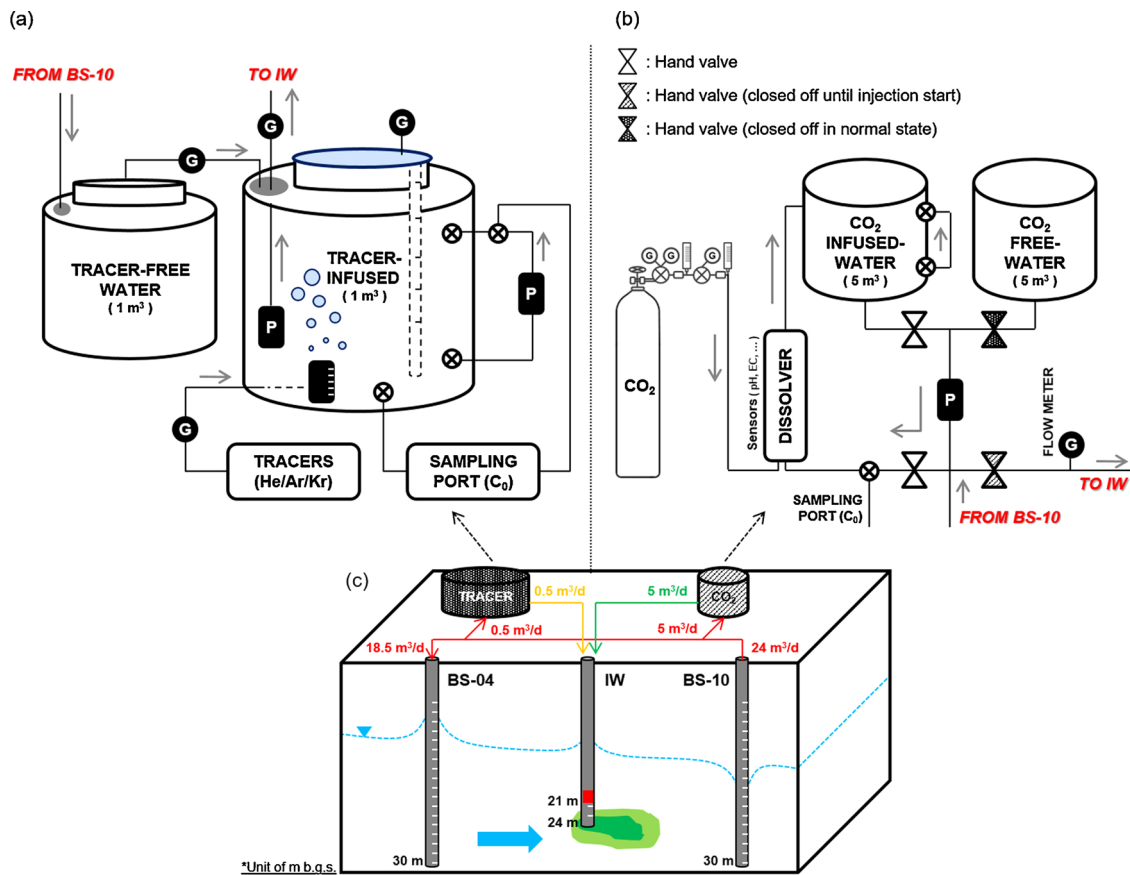


Fig. 2. Injection systems for the artificial CO₂ release experiment. (a) tracer-infused groundwater was prepared in a 1 m³ tank and (b) CO₂-infused groundwater was prepared in a 5 m³ tank. (c) gas-charged groundwater was continuously released into the induced pressure gradient field through the IW.

21–24 m bgs) in an isolated zone below a packer (Fig. 2c). The ambient surface weather conditions during the injection event were 20.4–26.9 °C without precipitation. The injection rate was controlled by a submersible and controllable quantitative pump (model MP1, Grundfos, Denmark) at a constant rate of 5.5 m³/d (Fig. 2c).

2.3. Real-time monitoring

Real-time monitoring data was collected from 17 May 2017 to 13 October 2017 (Fig. 3). Over this period, hydraulic pressure (P), temperature (T) and electrical conductivity (EC) were measured in-situ using the LTC Levellogger Junior (Solinst, Canada) and the barometric state was monitored at the same time using the Barologger Edge (Solinst, Canada) at 10 min intervals.

2.4. Water sampling campaign

2.4.1. Baseline survey period

Water samples were collected using a Waterra Inertial Pump with PowerPack PP-1 (Wattera, Canada) to obtain baseline data before the CO₂ injection. The local baseline of the pCO₂ was obtained on two occasions through water sampling between 16 June 2017 and 26 June 2017 (Fig. 3). The baseline for the noble gas tracers was determined by a single water-sampling operation on 26 June 2017 (Fig. 3). Alkalinity was determined in the field site by acid titration method with 0.05 N HNO₃. The pH and temperature were also measured in-situ using a portable water quality meter (YSI ProDSS, YSI Inc./Xylem Inc., USA). The noble gas samples were collected using a standard copper tube of 28 cm³ and a pinch-off clamp set.

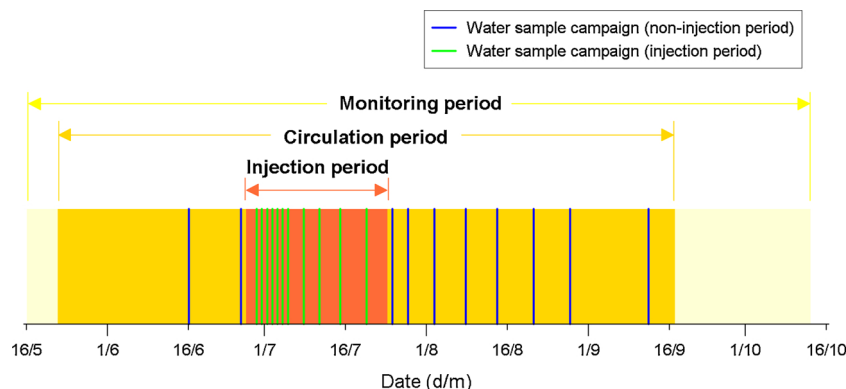


Fig. 3. Schedule for water sample collection during the CO₂ injection test.

2.4.2. Injection and post-injection period

Data acquisition after the CO₂ injection was conducted in the same manner as the baseline data collection. Water samples were collected on 19 occasions following the injection event, over 76 days from 27 June 2017 to 12 September 2017 (Fig. 3).

2.5. Laboratory analyses

2.5.1. Noble gas

The noble gas samples were analyzed in the noble gas analysis laboratory at the Korea Polar Research Institute (KOPRI) using an automated system as outlined in Stanley et al. (2009) and Kim et al. (2016). Gases were first extracted from a groundwater sample under high vacuum condition ($\sim 10^{-7}$ mbar) and stored in an aluminosilicate glass ampoule (Lott and Jenkins, 1998). Excessive water vapor, active gases, and condensable gases were then removed using cryogenic traps and a series of hot and cold Zr-Al alloy getters (St 101, SAES Getters S.p.A., Italy) before sample injection into the RGA200 mass spectrometer (Stanford Research Systems, California, USA) for analysis. The noble gases, He, Ne, Ar, and Kr were calibrated against air standards of 0.9 and 2.7 cm³ STP, to cover the wide range of the tracer enhanced injection water. The discrepancy between duplicate samples was less than 5% (Ju et al., 2019).

2.6. Analytical methods

2.6.1. pCO₂ calculation

pCO₂ values for the sampled waters were calculated using the monitored parameters of alkalinity, pH, and temperature. Alkalinity, pH and temperature were measured in-situ. Using these data a robust calculation for pCO₂ value was made using the program PHREEQC Version 3 (Parkhurst and Appelo, 2013).

2.6.2. Mass balance model

At the early stage of the CO₂ injection, the CO₂ plume is unstable with a high partial pressure, resulting in a degree of CO₂ degassing. Hence, CO₂ bubbles rise freely from the brine with a proportion of the CO₂ remaining in the dissolved phase. During the degassing period, the free-phase CO₂ strips out the dissolved, relatively insoluble noble gases, especially the lighter elements (He and Ne), leaving the system relatively enriched in the heavier noble gases (Ar, Kr, Xe) (Ballentine et al., 2002; Holland and Gilfillan, 2013). Based on the degree of this enrichment, we can inversely constrain the mass balance of the CO₂ plume in terms of the degassing process (see the Appendix A mass balance model for detailed explanation).

3. Results

3.1. Prior to CO₂ injection

Pressure and temperature changes result in the degassing of insoluble substances from the groundwater system. At the K-COSEM test site, the groundwater level shows a clear decreasing trend due to large-scale water consumption from nearby industrial complexes (Fig. 4) (Ju et al., 2019). However, prior to the experiment the hydrostatic pressure data showed a stable correlation with atmospheric pressure changes and no irregular turbulence (Supplementary Figure S1). Groundwater temperatures corresponded to normal seasonal values ranging between 12.7–13.6 °C (Fig. 4).

The induced pressure gradient commenced on the 22 May 2017 as a result of the onset of water circulation (Fig. 3c). Perturbations were detected in the water level (WL), temperature (T), and electrical conductivity (EC) values during the initiation of water circulation (see the start points of dark grey zone in Fig. 4). The pressure turbulence was most noticeable within the monitoring wells located inside the radius of influence (ROI) area both of the pumping (BS-10) and injection wells

(BS-04). For example, PS-04, SMW 1 series and SMW 2 series wells showed an instant pressure increase after the circulation commenced, as they are located near the injection well (BS-04) (Fig. 4d–j). In contrast, wells SMW 3–2 and 4–3 showed an abrupt decrease in pressure, as a result of their location near to well BS-10 where water was extracted (Fig. 4k and l). Well BS-09 also displayed a modest increase in pressure 9 days after water circulation commenced (specifically on 31 May 2017) (Fig. 4c). Temperature within all monitoring wells showed an overall increase after the water circulation regime started (see the start points of dark grey zone in Fig. 4). This is most likely linked to the groundwater for injection having resided in the surface tank at temperatures warmer (i.e., 17.1–28.6 °C) than those of the subsurface groundwaters (i.e., 13.3 °C) for the day prior to re-injection into the subsurface. The EC showed the overall decreasing trend in the initial circulation period as the re-injected water (BS-10) has a relatively low EC background compared to the other wells, with the exception of well SMW 2–1 (Fig. 4).

As outlined previously, two water sampling campaigns were conducted during the circulation period and prior to CO₂ injection commenced, in order to establish the groundwater baseline composition (16 June 2017 and 26 June 2017) (Fig. 3). The baseline alkalinity values were relatively low (27.5–64.1 mg/L), DO exhibited a wide variation (3.6–8.0), pH was weakly acidic (6.5–7.1) and pCO₂ was relatively low (0.0–0.01 atm) prior to CO₂ injection (Fig. 5). All of the parameters were close to the baseline values of low carbonate levels in the biotite granite protolith (Ju et al., 2019).

During the water circulation period, pH exhibited an overall decreasing trend as the low-pH water was pumped out from the down-gradient well (BS-10) and reinjected into the up-gradient well (BS-04) (Fig. 5c). DO also exhibited a decreasing trend as groundwater was re-equilibrated in the warm surface temperature (17.1–28.6 °C) before being injected into the well BS-04 (Fig. 4d). pCO₂ and alkalinity showed minor variation across the monitored region depending on the groundwater flow direction and the initial C parameter distributions (Fig. 4a and b).

Mean He, Ar and Kr concentrations measured before the injection commenced were 5.43×10^{-8} cm³ STP/g_{H₂O}, 3.72×10^{-4} cm³ STP/g_{H₂O} and 9.80×10^{-8} cm³ STP/g_{H₂O}, respectively. These are close to the Air Saturated Water (ASW) value at the temperature condition (i.e. 13.3 °C) of study site—such as 4.58×10^{-8} cm³ STP/g_{H₂O}, 3.58×10^{-4} cm³ STP/g_{H₂O} and 8.30×10^{-8} cm³ STP/g_{H₂O} for He, Ar and Kr values, respectively (Kipfer et al., 2002).

3.2. Injection fluid

The gas-infused groundwater was released into the IW from 27 June 2017 to 24 July 2017 (Fig. 3). The CO₂-infused groundwater (C₀) collected from the 5 m³ tank (Fig. 2b) was initially below the saturation point (0.40 atm) for 11 days after the injection (29 June 2017 to 8 July 2017), and reached to the over-saturation state (> 2.3 atm) about 18 days after the injection on 15 July 2017 (Fig. 5a). This CO₂ variation can be attributed to an accidentally reduced water flux going into the CO₂ tank, causing a decrease of the water level, resulting in altering of the C system balance in CO₂ tank. For the same reason, the pH and DO initially maintained 5.0 and 3.9 mg/L but showed a sudden decrease to 4.2 and 0.5 mg/L on the 15 July 2017. Water samples collected from the 1 m³ tank (C₀) (Fig. 2a) were analyzed for their He, Ar and Kr concentrations, and reported at 2.92×10^{-5} cm³ STP/g_{H₂O}, 2.26×10^{-2} cm³ STP/g_{H₂O} and 4.95×10^{-5} cm³ STP/g_{H₂O}, respectively. The noble gas concentrations lie between fully saturated and Air Saturated Water (ASW) levels, and thus they will remain dissolved in the groundwater system unless being exposed to low partial pressure conditions such as air bubbles or the vadose zone interface (i.e. water table) (Ju et al., 2019).

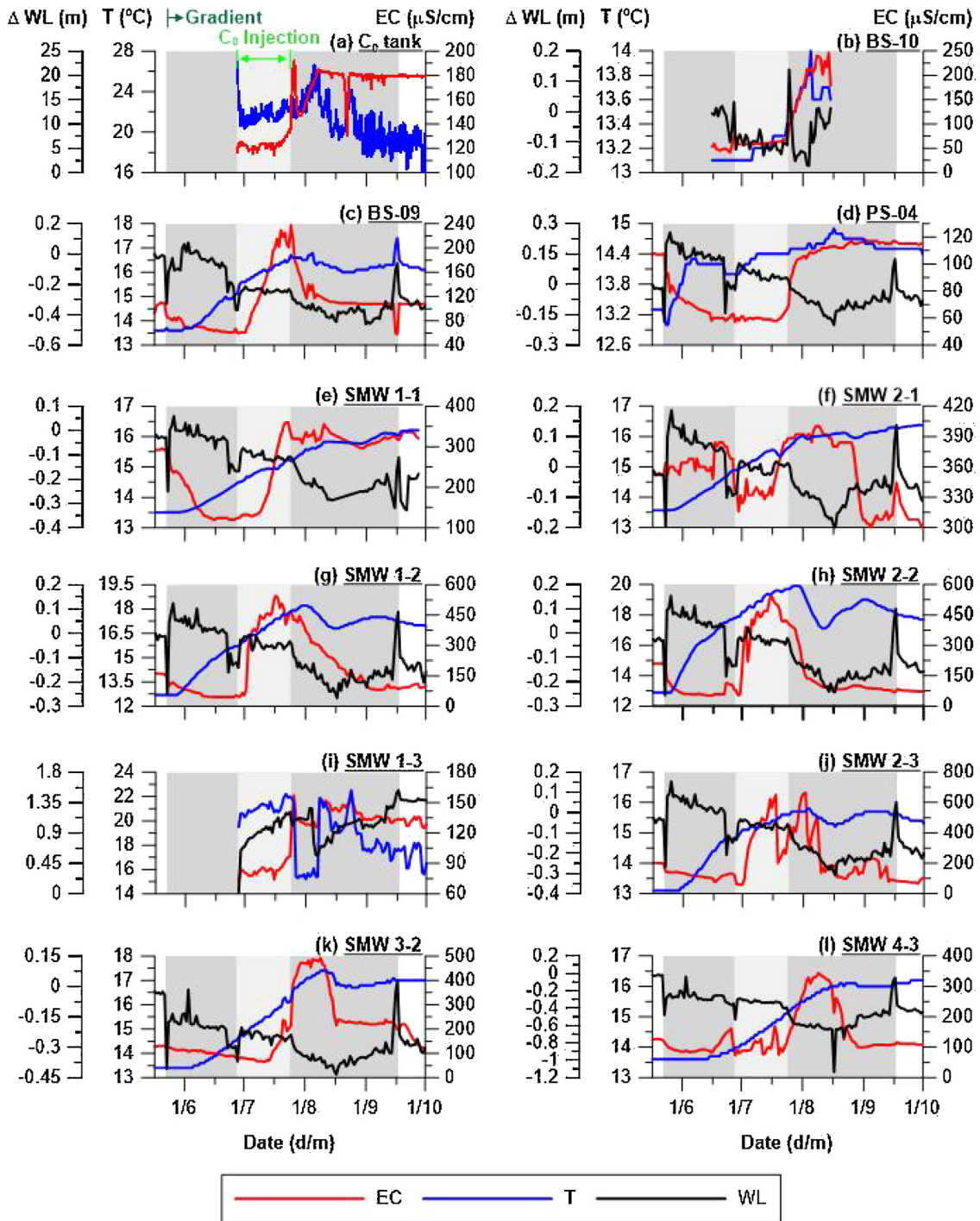


Fig. 4. Water level (WL), temperature (T) and electrical conductivity (EC) data. Measurements were completed in the monitoring wells continuously using a LTC data logger. The groundwater circulation was initiated at 22 May 2017 (dark grey shaded zone) and the CO₂ injection started at 27 June 2017 and kept going till 24 July 2017 (light grey shaded zone).

3.3. Post injection

3.3.1. P, T and EC

Pressure turbulence was observed in all monitoring wells prior to the initiation of CO₂ injection (Fig. 4), which can be attributed to the change in water volume from 24.0 m³/d to 18.5 m³/d for preparing the gas-infused water of 5.5 m³ (C₀) before CO₂ injection within the circulation system (see the section 2.2.2 Injection for detailed explanation). Minor changes in temperature were observed inside the Radius of Influence (ROI) zone of IW such as PS-04, BS-09, SMW 1 and SMW 2

(Fig. 4c–j). The temperature showed a gradual increase since the groundwater circulation initiated in which the SMW 2–2 showed the highest increase of up to +7.0 °C and followed by SMW1–2 (+5.5 °C), SMW 3–2 (+4.0 °C), BS-09 (+3.8 °C) and the others (< +2.8 °C) (Fig. 4). The relatively high increase in the temperature of BS-09 indicates a preferential flow gradient still exists in the study site even after the formation of the induced pressure gradient (Fig. 1a). In EC data, the most prominent signals were recorded at SMW 1–2 (+464 μS/cm, +472 %), SMW 2–2 (+447 μS/cm, +368 %), SMW 2–3 (+531 μS/cm, +301 %), SMW 3–2 (+383 μS/cm, +250 %) with the

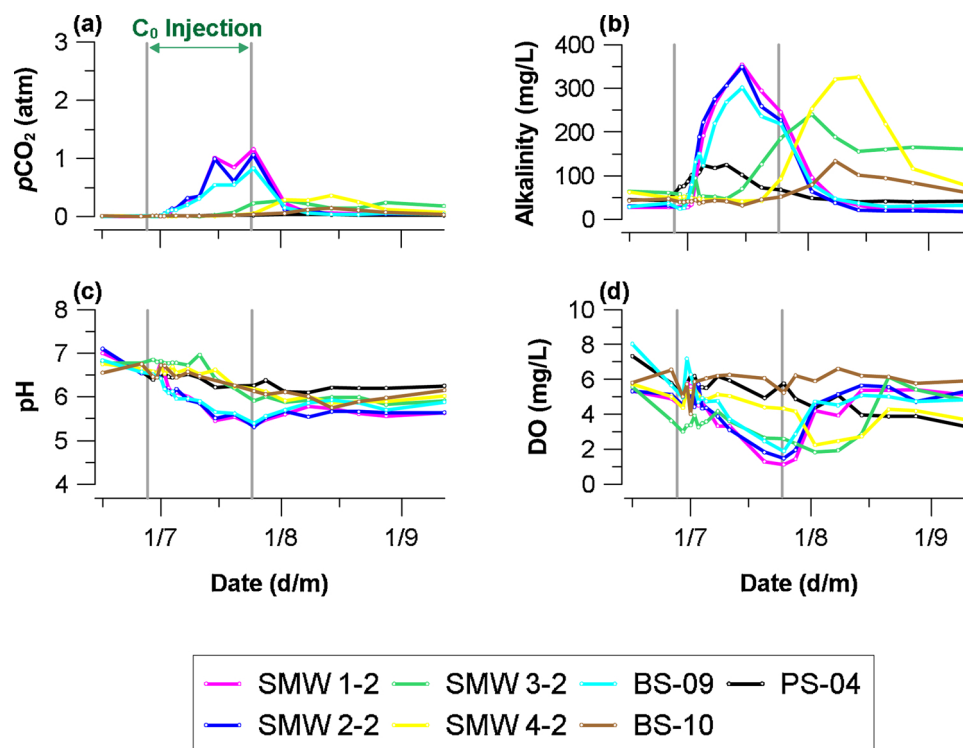


Fig. 5. pCO_2 , pH, alkalinity and DO values. The grey vertical lines represent the injection period.

others showing a less pronounced change ($< +129\%$). These observations were consistent with temperature data, exhibiting the greatest change in the SMW #–2 wells. This indicated that the CO_2 plume moved horizontally from the injection depth of 21–24 m to the screen depth of SMW #–2 (i.e., 20–22 m) (Fig. 1c). The response in EC is clearly different to that of temperature as a notable increase in EC was only observed after CO_2 injection occurred. This is because EC is the function of geochemical interaction between the CO_2 water and the rock materials (Vialle et al., 2014). In the groundwater flow regime, the SMW series wells, BS-09 and BS-10 are located ahead of the migration direction of the IW, which is illustrated by the clearly increasing EC trend (Fig. 1b). Alternatively, well PS-04 is located upgradient from the CO_2 injection point, resulting in a gradual lowering of the EC trend after the CO_2 injection was initiated as there is no communication between this well and the CO_2 rich-water (Fig. 1b).

3.3.2. pCO_2 , pH, alkalinity and DO

As expected, the chemical elements exhibited strong signals correlating with the CO_2 plume arrival. The parameters are presented as breakthrough curves (BTCs) (Fig. 5). Note that for the SMWs, the parameters represent the data from the injection depth (i.e., SMW #–2) only, as this generated the largest signals among all depths. The pCO_2 produced the strongest signal at SMW 1–2 (+1.15 atm, +25,385 %) which was followed by SMW 2–2 (+1.05 atm, +18,067 %), BS-09 (+0.82 atm, +12,631 %), SWM 4–2 (+0.35 atm, +3,746 %) and the other wells ($< +2,923\%$) (Fig. 5a). The pronounced response of pCO_2 compared to other parameters is attributed to its low baseline concentration (0.0–0.01 atm) (Risk et al., 2015). Alkalinity also showed significant increases with the arrival of the injected CO_2 , particularly in wells SMW 1–2 (+326.4 mg/L, +1,189 %), SMW 2–2 (+318.0 mg/L, +1,017 %), BS-09 (+269.2 mg/L, +821 %), SMW 4–2 (+270.0 mg/L, +478 %) with other wells showing smaller, but measureable changes ($< +286\%$) (Fig. 5b). Alkalinity gradually increases with the chemical interactions between the CO_2 plume and the aquifer materials similar to the EC. The small differences in response to CO_2 injection between EC and alkalinity can be attributed to the geochemical variation of the

study site resulting in different CO_2 related buffering capacities (Sechriest, 1960).

The pH also decreased noticeably, changing by -1.5 units at SMW 2–2, which was followed by -1.5 units at SMW 1–2, -1.4 units at SMW 2–3, -1.3 units at BS-09 and > -0.96 units at the others (Fig. 5c). The DO showed relatively modest change by up to -4.0 mg/L (-78 %) at SMW 1–2 which was followed by BS-09 (-4.9 mg/L, -72 %), SMW 2–2 (-3.7 mg/L, -72 %), SMW 3–2 (-2.8 mg/L, -60 %) and the others ($< -58\%$) (Fig. 5d). In this experimental setting, the DO evolves with the three-component groundwater mixing between low-DO water volumes (re-injection water at BS-04 and injection water at IW) and high-DO water volume (local groundwater) (Fig. 2).

3.3.3. Noble gas tracers

The measured concentrations of He, Ar and Kr tracers are presented in BTCs (Fig. 6). The concentration was normalized to the injection amount (C_0) after the background portion (i.e. atmospheric origin) was subtracted from both monitored (C) and initial concentration (C_0), to simply define the CO_2 arrival as a positive signal. Note that for the SMWs, the parameters present the data from the injection depth (i.e., SMW #–2) only, as this exhibited the largest signals of all depths. As a result, the tracers successfully produced the strong positive signals with the CO_2 plume arrival in the BTCs (Fig. 6). The tracer concentrations exhibited variable arrival times and concentrations due to the CO_2 plume following different flow paths within the heterogeneous groundwater system at the site, similar to the findings of Kilgallon et al. (2018); Lee et al. (2017); Lu et al. (2012) and Stalker et al. (2015). Most importantly, Kr showed the earliest arrivals through all monitoring wells compared to the He and Ar tracer. This was attributed to the Kr taking a less distributed pathway through the subsurface than the other tracers, and a result of the dilution of CO_2 plume along the concentration gradient (see the discussion section 4.1.2 Diffusion process controlling the efficiency of noble gas tracing).

The tracers associated with the CO_2 plume were firstly detected in SMW 2–2 (+4 d) followed by BS-09 (+4 d), SMW 1–2 (+5 d), SMW 3–2 (+18 d) and SMW 4–2 (+23 d) (Fig. 6a, c, d, e and f). The

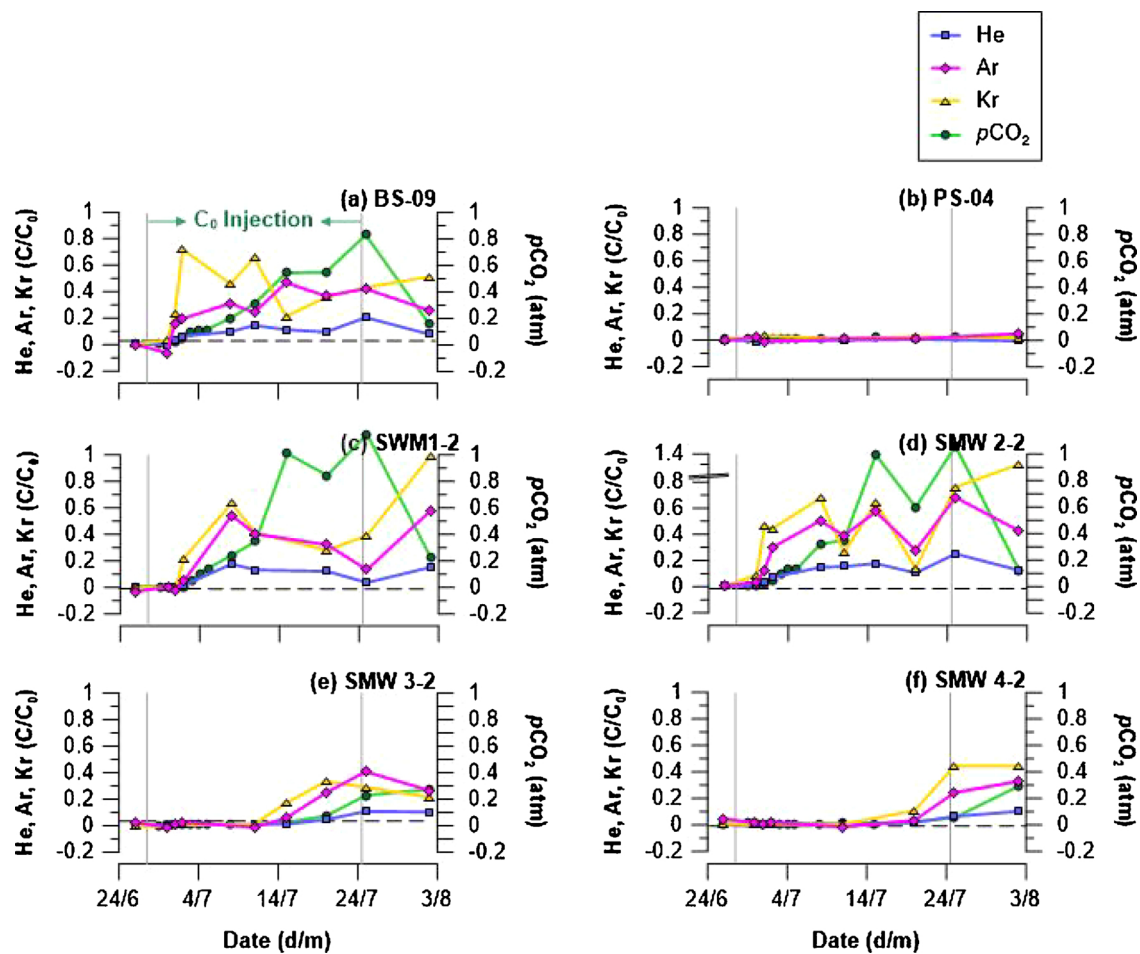


Fig. 6. Gas tracer concentration during the experiment. Noble gas was presented as C/C_0 (see the text for details) with pCO_2 (atm). The grey vertical lines show the start and end of the injection period. The Air Saturated Water (ASW, black dotted horizontal line) was calculated according to Kipfer et al. (2002) to indicate the local background level of noble gas tracers.

strongest signal was recorded at SMW 2–2 (+1,430 % for He, +322 % for Ar and +6,904 % for Kr) suggesting the majority of the CO_2 plume moved along the induced groundwater pressure gradient (Fig. 6). A portion of the tracers also moved toward BS-09 and produced a strong signal in spite of being a greater distance away from the injection point (5.2 m) than that of SWM 1–1 and SMW 2–2 (2.6 m). This can be attributed to the preferential flow pathway present in the study site (Fig. 1a) (Ju et al., 2019; Lu et al., 2012). Well PS-04 did not record the presence of any tracers during the injection period due to its location behind the IW in the groundwater flow direction (Fig. 1b). It is worth noting that SMW 4–2 exhibited a higher concentration of Kr once the tracers arrived than SMW 3–2 (Fig. 6), implying that a low conductivity zone hinders well SMW 3–2 from capturing the full CO_2 plume. This result was consistent with the observations made in alkalinity and pCO_2 (Fig. 5).

As the injection water gradually approached the monitoring network, the observation wells captured the temporal evolution of the CO_2 plume. In the early stage of BTCs, Kr showed the fastest arrival time compared to the other tracers for all monitoring wells (Fig. 6). This was followed by an increase in Ar and He concentrations, with both parameters soon reaching their peak concentration within a few days (Fig. 6). In the final stage of BTCs, the plume tail is recorded in all of the monitoring wells through the decrease of noble gas concentrations after injection at the IW ceased. However, it can be observed that the concentration increased in the last stage of the BTCs for monitoring wells adjacent to IW (Fig. 6c and d). This can be attributed to the circulation injection system of this experiment. In the final stage of the injection

period (4 days before the end of injection), the tracer-charged plume had reached BS-10 (Fig. 4b). As water was still being produced for the reinjection at the IW, a portion of the CO_2 plume was returned back into the injection tank containing the artificial noble gas tracers. Note that heavier components such as Ar and Kr acted as an early warning tracer for CO_2 arrival in every monitoring well during the monitoring period. This was attributed to physical mechanisms affecting the distribution of the dissolved gases (see the section 4.1.2 Diffusion process controlling the efficiency of noble gas tracing).

The consistent temporal evolution of the recorded noble gas concentrations within the six monitoring wells is depicted in the ternary diagram of Fig. 7. The local BG (i.e., green star) represents the average of background level of individual monitoring wells. Prior to the CO_2 plume arrival, each monitoring well plots near to the Air Saturated Water (ASW) level. The initial arrival of the CO_2 plume was marked by a significant increase in Kr in all monitoring wells (see the arrow 1 in Fig. 7) which corresponds to the early stage evolution in the BTCs (Fig. 6). Note that PS-04 did not exhibit a response after injection. Following the arrival of the Kr tracer, the He and Ar concentrations within the monitoring wells increase as the plume center approached, converging at a single point (Fig. 7). However, the concentrations of noble gas tracers at the peak concentrations were lower than those at the time of injection. They were 73.6–88.3 % (He), 26.2–55.5 % (Ar), and 0–65.5 % (Kr) of the initial concentrations. The lower concentrations can be attributed to the degassing loss of the injection fluid (Sathaye et al., 2016), explained in more detail in the section 4.1.1. This degassing process controls the overall retention amount of the injected

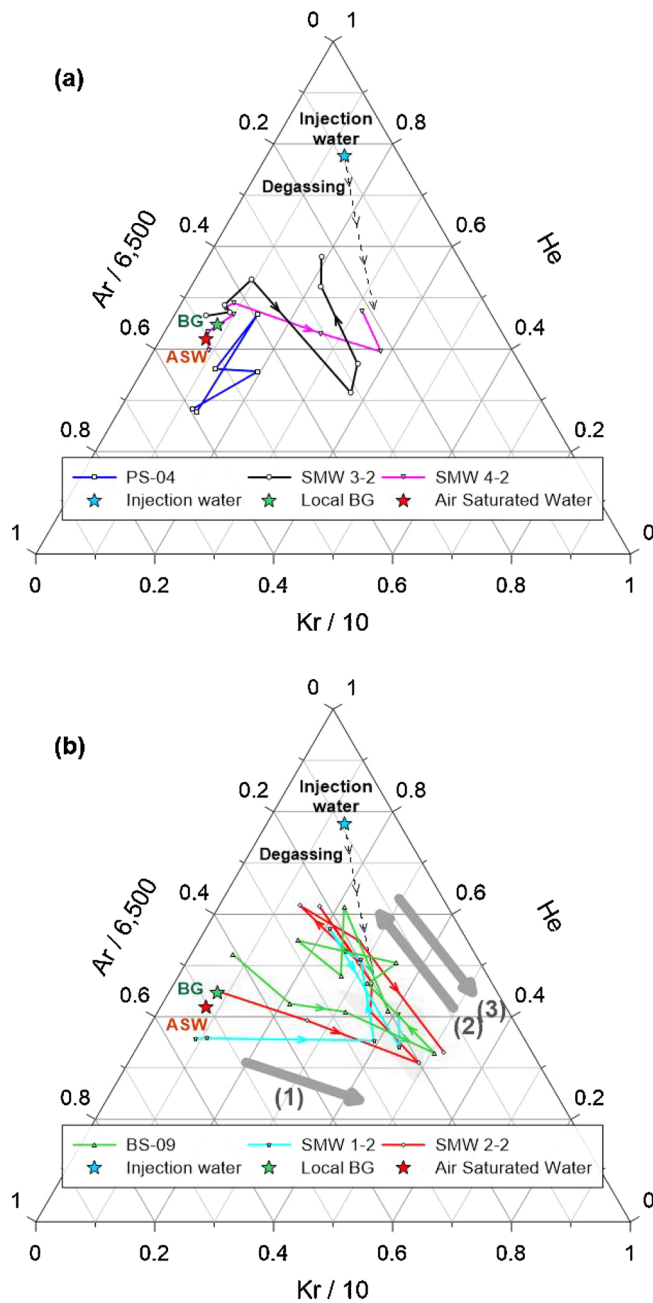


Fig. 7. Noble gas ternary diagram showing the two groups of wells categorized by their response. (a) monitoring wells which showed no concentration change from background level (i.e., PS-04) or only an early-stage evolution (i.e., SMW 3-2 and SMW 4-2). (b) monitoring wells that showed a three-step evolution as located close to the injection point (i.e., SMW 1-2 and SMW 2-2) and located in a preferential migration path (i.e., BS-09). The early-stage CO_2 plume is characterized by high Kr concentration (Arrow 1), the plume then gradually increases in He and Ar concentrations (Arrow 2). In the final stage, it becomes rich in Kr again, following the cessation of injection (Arrow 3). The peak composition was different from that of injection water due to initial degassing loss.

CO_2 . The composition of the plume tail captured in the monitoring wells was similar to the composition of the plume front, characterized by a high Kr concentration (Fig. 7).

3.4. Following injection

CO_2 injection ceased after 28 days (27 June 2017 to 24 July 2017)

(Fig. 3). This corresponds to the point where the monitoring parameters start to change at the BS-10 (Fig. 4b and 5). In this moment, the slight increase of EC was also observable in the CO_2 tank as CO_2 water re-entered the injection tank (Fig. 4a). Additionally, PS-04 also showed a minor increase in EC at the termination period due to the re-circulation of CO_2 injected water (Fig. 4d). From this point (24 July 2017), the groundwater circulation system was modified to avoid the re-enhancement of the CO_2 plume. Another local groundwater from BH-03 was prepared and from then onwards substituted the circulation portion going to the BS-04 (Figs. 1e and 2 c).

3.5. Following groundwater circulation

The groundwater circulation ended on 17 September 2017, 56 days after CO_2 injection stopped and 118 days after groundwater circulation commencement (Fig. 3). The pressure turbulence was observable in all monitoring wells (Fig. 4) and also EC turbulence was detected in some of the monitoring wells (Fig. 4c, f and k), but the groundwater quickly recovered to its previous state (Fig. 4).

4. Discussion

4.1. Mass retention mechanisms

4.1.1. Degassing process controlling the overall retention amount of released CO_2

If an inert tracer is continuously released into the groundwater system, the concentration will gradually increase in monitoring wells and eventually become similar to the composition of injection fluid. In this study, as the tracer-charged water was continuously released into the groundwater system, the monitored concentration was expected to resemble the injection fluid's concentration by the final stage. However, a notable difference in CO_2 and noble gas concentrations was observed between the injection fluid and the plateau points (Fig. 7). This phenomenon indicates that tracer mass was not conserved in the groundwater system and suffered from mass-reducing processes. As the noble gas tracer is biochemically inert in the groundwater system, the decrease is likely to be the result of physical processes (Holland and Gilfillan, 2013). For instance, a similar noble gas deficit has been observed in a natural CO_2 -rich system, where CO_2 and CH_4 bubbles also stripped out the insoluble gases from the groundwater system (Gilfillan et al., 2008, 2017; Brennwald et al., 2005; Zhou et al., 2005) and in artificial CO_2 injection sites (Nimz and Hudson, 2005; Stalker et al., 2015). Hence, this deficit could be explained by the degassing of unstable CO_2 -rich plume.

A diagram was constructed using noble gas tracers to determine the major processes influencing the CO_2 plume migration (Fig. 8). In Fig. 8, the concentrations of He and Ar at the well SMW 2-2 (on 25 July 2017) decreased gradually to their background concentration (BG_p), indicating mixing of the plume with the local groundwater. The mass distribution of observed samples was the function of two distinct processes over the testing period: mass reduction of the CO_2 plume occurred through the degassing process (black line), followed by the dilution of the plume by the local groundwater (black dotted line). The observed data clearly indicated the mixing process was preceded by the degassing process.

Elemental fractionation of noble gases is controlled by their differing solubilities and the ambient reservoir conditions (Fig. 8) (Ballentine et al., 2002; Ma et al., 2009). In a closed system, the dissolved air remains in the groundwater, and equilibrium is achieved between the bubbles and the surrounding groundwater. In an open system, the air bubbles are mobile after the phase transition and escape from the aquifer system continuously until the end of the degassing process. In Fig. 8, the mixing line (black dotted line) intersects a degassing line (black line) explaining the loss of air bubbles by $1.40 \times 10^{-2} \text{ cm}^3/\text{g}_{\text{H}_2\text{O}}$ through the degassing process in an open system. The

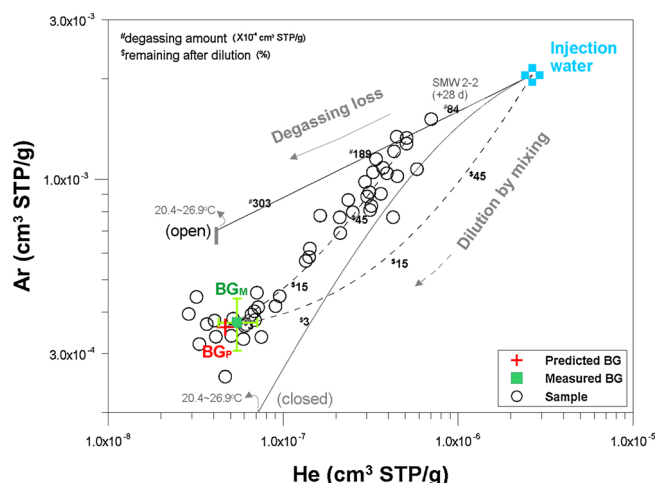


Fig. 8. Mass balance of the CO₂ plume depicted with He and Ar tracer. The plume was expected to follow the mixing line between the injection water (blue cross symbol) and the measured background concentration (BG_M, green square symbol). Degassing loss of CO₂ from the dissolved CO₂ plume, would result in a new mixing line starting from the SMW 2-2 (+28 days) toward the background concentration (BG_P, red cross symbol). The BG_P was estimated based on the optimization process of the degassing model (see the Appendix B Model optimization for detailed explanation). The shaded zone on the degassing models indicates the uncertainty arising from the injection water temperature (20.4–26.9 °C).

analytical technique for this calculation is shown in Appendix A Mass balance model. In the experiment, CO₂ degassing was detected just above the water table at the IW reconfirming the initial loss happened into the vadose zone (Supplementary Figure S2).

Unlike noble gases, CO₂ is involved in diverse chemical and biological processes in the groundwater. To identify the major controls on the CO₂ distribution, the *p*CO₂ was plotted against measured noble gas tracer concentrations in Fig. 9. As expected, the total mass of CO₂ in the plume was decreased by degassing and mixing processes. Our data designate a clear mixing line stretching from SMW 1–2 (25 July 2017) to BG_P, indicating that mixing process mainly controlled the mass distribution of CO₂ in the plume after the initial degassing event. The minor variations from the mixing trend mostly fall in the ranges of the initial composition of injected CO₂-infused water (Fig. 9). The solubility-controlled process is shown as the black arrow stretching from the blue-cross symbol to red-cross symbol (Fig. 9). The abrupt change in He/Ar ratio stands in strong contrast to the minimal change observed in the *p*CO₂ during the degassing event (ca. 1.6 % overall loss of CO₂). Losses of noble gases (20.5 % for Kr, 34.0 % for Ar, and 80.1 % for He) are much greater than for CO₂ (Table 1).

4.1.2. Diffusion process controlling the efficiency of noble gas tracing

The different noble gas species cover a wide mass range and thus may provide a chance to constrain the mass-dependent processes occurring in the groundwater system. A comparison was made to scrutinize the behavioral difference for noble gases, as observed from the He/Ar (Fig. 8) and He/Kr (Fig. 10) relationships. The mixing line in Fig. 10, represented by a black dotted line stretching from the degassing line to BG_P, corresponds to the mixing line estimated in Fig. 8. However, it is noteworthy that the He and Kr pair did not exhibit a singular trend with many variations scattering from the estimated mixing line. It is also noteworthy that samples from the plume's center tend to converge on the estimated mixing line, while the samples from both the plume's front and tail display a large scatter pattern over the estimated line

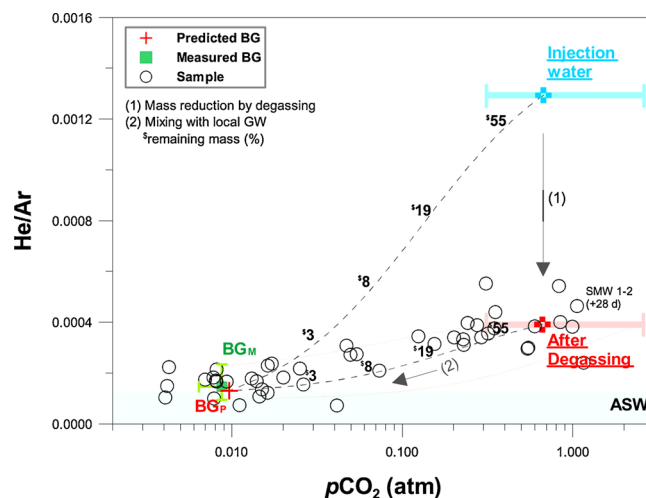


Fig. 9. Plot of *p*CO₂ against He/Ar showing the concentration changes of CO₂ and noble gas tracers during CO₂ plume evolution. The BG_M (green square symbol) is the measured background level, and the BG_P (red cross symbol) is an estimated value from the optimization process of the degassing model (see the Appendix B Model optimization for detailed explanation). The CO₂ plume firstly reduces total mass by the degassing process (Arrow 1) and then gradually gets diluted by mixing with local groundwater (Arrow 2).

(Fig. 10). Such discordance was also observable in the *p*CO₂ versus He/Kr diagram (Fig. 11) in which many samples, especially those from the plume's front and tail had significantly lower He/Kr ratios (around 0.10) than the ratio describing the estimated mixing line (0.24). This difference indicates that another mass-dependent process was affecting the tracer distribution in addition to the solubility-controlled process.

To further examine the temporal progression of the CO₂ plume, ternary plots of *p*CO₂, He, and Ar or Kr were composed according to the locations of samples in the plume (i.e., front, center, and tail) (Fig. 12). In the He/Ar/*p*CO₂ diagram, the samples have a small variation near BG_P in the initial period, while as the plume center approached the monitoring points, it showed an upward shift toward the degassing point in the Fig. 12a. In the He/Kr/*p*CO₂ diagram, the samples show a much wider variation during the initial stage of the CO₂ plume arrival than the observed change in the He/Ar/*p*CO₂ diagram (Fig. 12b). This difference indicated that another physical process was involved in the mass distribution at the CO₂ plume's front. Note that the initial composition of the plume was characterized by the high concentration of Kr as it appeared firstly in the observation wells (see also Fig. 7).

In open water, diffusion is capable of elemental fractionation depending on the molecular mass (Zheng and Bennett, 2002). According to Fick's law, the mass distribution of a solute in a groundwater system is restricted by molecular diffusion along the concentration gradient. In our experimental design, the artificial injection formed a CO₂- and tracer-rich plume in the groundwater system, setting a steep concentration gradient at the plume boundary. Consequently, the plume boundary was actively subjected to the diffusion process facing with the local groundwater of low concentration level of noble gases. As the diffusion rate is inversely proportional to the elemental mass of the solute, the tracer composition at the plume boundary was regulated by the mass-dependent fractionation. This phenomenon also has been observed in a coal bed methane field, where the free CO₂ and CH₄ gases stripped off the insoluble noble gases from groundwater and this action set the concentration gradient at interfaces with the un-degassed local groundwater, at which diffusion process resulting in a mass dependent fractionation of noble gas tracers (Zhou et al., 2005). Overall, the fact

Table 1
Mass balance of the leaked CO₂ plume in shallow aquifer system.

| Open system | Injection | | After degassing loss | | | Solubility [†] (mM/atm) |
|---------------------------------|-----------------------|------------------------|-----------------------|-------------------------|---------------|-------------------------------------|
| | Amount (kg) | partial pressure (atm) | ΔAmount (kg) | Δpartial pressure (atm) | Remaining (%) | |
| He | 7.04×10 ⁻⁵ | 3.07×10 ⁻⁶ | 5.64×10 ⁻⁶ | 2.46×10 ⁻⁶ | 19.9 | 0.386 |
| Ar | 5.43×10 ⁻⁵ | 6.11×10 ⁻⁶ | 1.85×10 ⁻⁶ | 2.08×10 ⁻⁶ | 66.0 | 1.50 |
| Kr | 2.50×10 ⁻⁵ | 7.41×10 ⁻⁶ | 5.13×10 ⁻⁶ | 1.52×10 ⁻⁶ | 79.5 | 2.71 |
| CO ₂ p. [*] | 1.70×10 ² | 6.62×10 ⁻⁶ | 2.72×10 ⁻⁶ | 1.07×10 ⁻⁶ | 98.4 | 38.7 |

[†] NIST chemistry webbook of Sander (2017) at temperature of 21.8 °C.

^{*} The predicted value from model optimization (see the Appendix B Model optimization for detailed explanation).

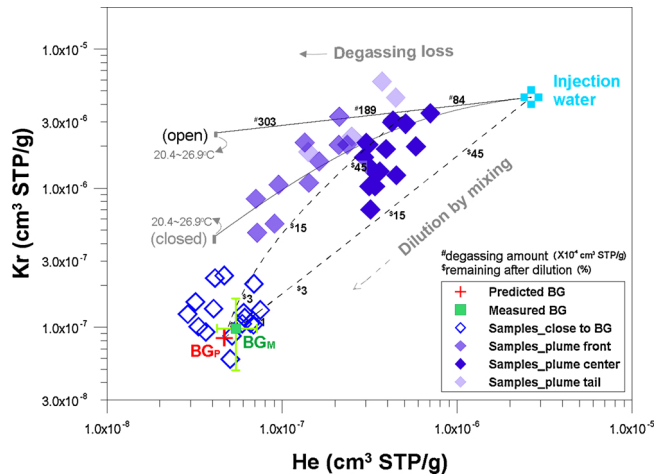


Fig. 10. Mass balance of the CO₂ plume depicted with He and Kr tracers. To see the plume evolution in detail, the samples were sorted by the breakthrough positions. Note that many samples, especially on the plume front and tail, are scattered over the estimated mixing line, contrary to the He–Ar pair mixing trend in Fig. 8.

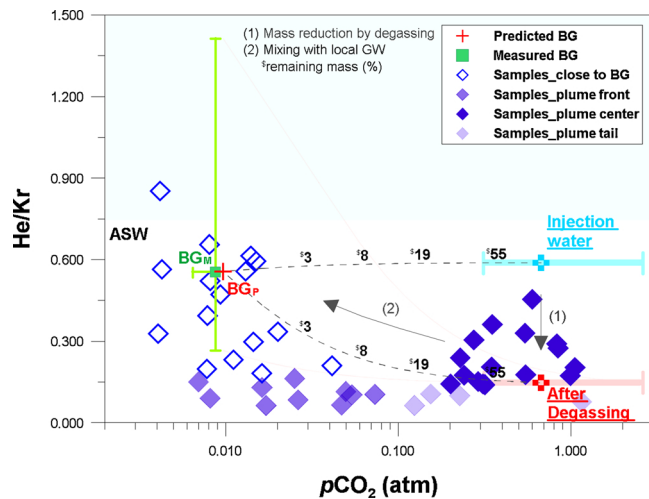


Fig. 11. Diagrams showing the concentration changes of CO₂ and noble gas tracers during CO₂ plume evolution. To see the plume evolution in detail, the samples were sorted by the breakthrough positions. Note that, many samples, especially on the plume's front and tail, are scattered from the estimated mixing line, as compared to the observations in the pCO₂ versus He/Ar relationship in Fig. 9.

that the diffusion allocates the mass distribution at plume boundary (i.e., plume's front and tail) suggests that the early detection of the migrated CO₂ plume is dependent on this process. This further implies that the early-stage degassing loss is of primary importance in terms of

the noble gas tracing efficiency because the degassing process is associated with the overall plume composition including the feature of the concentration gradient at plume front.

5. Conclusions

A portion of CO₂ stored within the deep subsurface may unintentionally migrate upward to reach overlying shallow aquifers. Whilst noble gas tracers have proved to be useful in monitoring CO₂ leakage, they have been rarely adopted for monitoring purposes in the shallow aquifer system. This study utilized the noble gas tracers to indicate the CO₂ leakage and also to elucidate the mass balance of the leaked plume after injection of 1.70 × 10² kg of CO₂ into a shallow aquifer system. The CO₂- and tracer-enhanced groundwater was released into the induced gradient field and subsequent monitoring works have been conducted. The noble gas tracers produced a strong signal of the migrated CO₂, with Kr consistently exhibiting the first arrival time, ahead of the plume and the other noble gas tracers throughout all of the monitoring points.

The mass distribution of the CO₂ plume was controlled by three different physical processes; solubility-controlled (degassing), physical groundwater mixing and diffusion. The degassing process reduced the overall mass of the CO₂ plume and caused noble gas tracers to be mass-dependently fractionated, which occurred at the initial stage of CO₂ leakage before plume migration. The diffusion process was also involved during the plume migration, but only influenced the noble gas distributions in the leaked plume and did not act as a primary control for the CO₂ distribution within the monitoring period. This phenomenon, however, can accelerate the dilution of artificial tracers at the plume front, especially for the lighter elements, suggesting this process has an important control on the monitoring efficiency of the artificial tracers in terms of early detection of CO₂ leakage. Most importantly, as the noble gas tracers display more apparent changes according to the retention mechanisms than CO₂ itself, they can provide a robust system for precisely monitoring both the fate and pathway taken by the migrating CO₂.

Noble gas tracers were used to constrain the physical retention mechanisms of the injected CO₂ within a shallow aquifer. Our findings indicate that around the injection point, CO₂ degassing dominantly occurs from the dissolved plume due to the high gas pressure, suggesting a near-surface monitoring network is necessary for capturing the active “vertical” movement of degassed budget in this area. This can be accomplished by performing a continuous monitoring of CO₂ at the vadose zone, for example by a soil flux measure, soil gas sampling and borehole head space sampling around a potential leak point. The monitoring regime can be performed cost-effectively with limiting a “degassing boundary” around a suspected leak point. In this study, only a few meters away from the leak point (> 2.6 m), the degassing behavior was greatly diminished as a gas pressure of CO₂ plume reduced significantly. From this point, the CO₂ plume was stabilized as a dissolved phase and dominantly diluted by mixing with a local groundwater along a flow direction. Therefore, from this stage, sparse monitoring of saturated zone is recommended for tracing down a horizontal

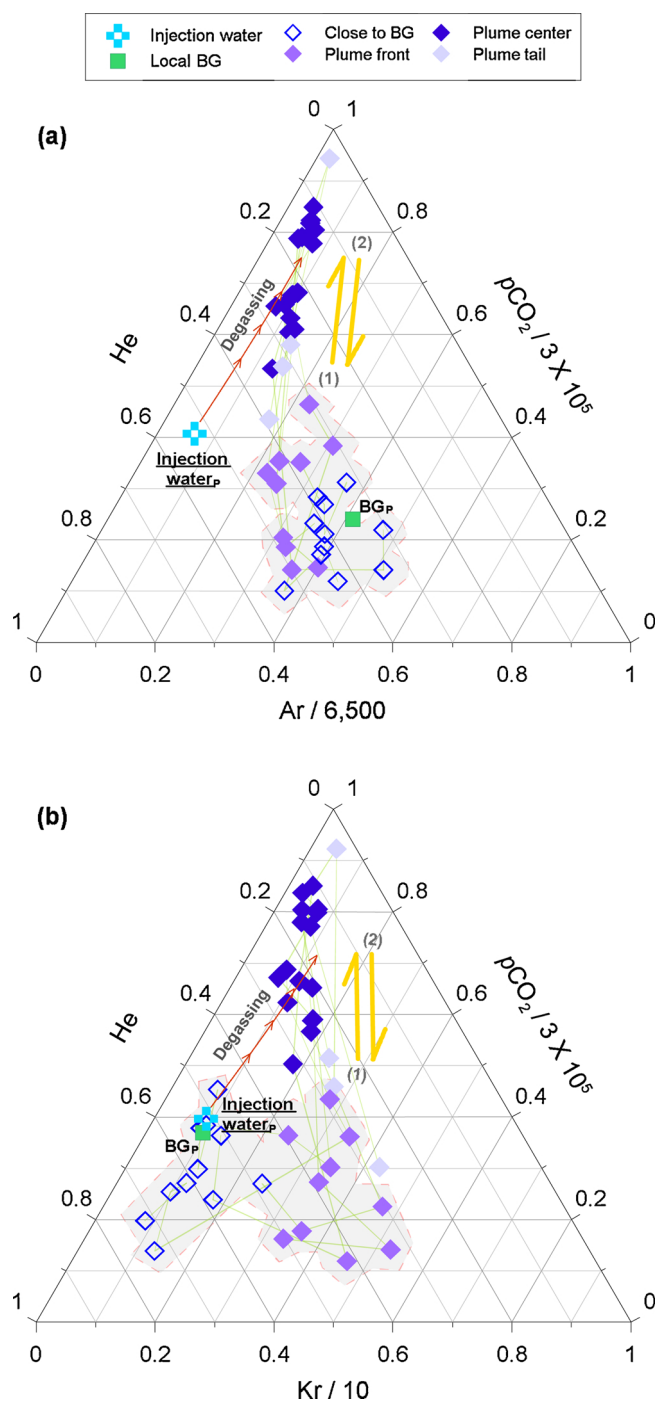


Fig. 12. Ternary diagram showing the compositions of $p\text{CO}_2$, He, and Ar (a) or Kr (b) tracers. To scrutinize the plume evolution, the samples were sorted according to the breakthrough positions. In the initial period of plume evolution, the relative compositional change among $p\text{CO}_2$, He and Kr (b) showed a much wider variation near the background levels (BG_p , green square symbol) than that observed among $p\text{CO}_2$, He and Ar (a), which attributed to the diffusion process (see the text for details). This diffusion-dominant movement was followed by the upward shift toward the degassing point (see Arrow 1), as also shown by the intersection point in Fig. 8. In the final stage, the samples return to the composition similar to the plume front (see Arrow 2), after cessation of injection.

migration of a dissolved CO_2 plume, rather than an intensive gas monitoring for a degassed component. Hence, the key aspect to establish an effective monitoring network is how well constrained the “ CO_2 degassing boundary” around a potential leak point is, and how well the groundwater flow regime is understood.

Monitoring of degassed CO_2 might not be easily achieved in a real CCS field using direct measurements. In this study, the degassing boundary was just a few meters from the leak point (< 2.6 m), whilst a strong artificial gradient (~ 0.18) was enforced for the plume migration. This suggests that a degassing boundary would be even narrower in a natural gradient system, making a direct detection of this extremely difficult. Furthermore, heterogeneity in the vadose zone can put an additional uncertainty in monitoring of the vertical flux, as gaseous CO_2 can take various pathways in the vadose zone depending on the soil permeability distribution (Cohen et al., 2013). Hence, identification of a point source of CO_2 leakage using a direct measurement technique in the vadose zone would be very difficult, unless an intensive monitoring is undertaken around the exact point source. However, noble gas monitoring of groundwater is able to record the migration of a CO_2 plume from the leak point along the groundwater flow pathway, as highlighted in this study. Our findings are similar to previous work (Mackintosh and Ballentine, 2012) that showed monitoring of noble gases in groundwater is an order of magnitude more sensitive for detecting migrated gases than vadose zone gas monitoring. Therefore, we recommend that monitoring of noble gases in groundwaters should be used in addition to direct vadose zone methods, in order to increase the sensitivity of the monitoring regime and improve the protection of the shallow groundwater aquifer above a storage site.

CRediT authorship contribution statement

YeoJin Ju: Conceptualization, Methodology, Data curation, Investigation, Writing - original draft. **Stuart M.V. Gilfillan:** Writing - review & editing. **Seong-Sun Lee:** Project administration, Investigation. **Dugin Kaown:** Data curation. **Doshik Hahm:** Resources, Data curation, Writing - review & editing. **Sanghoon Lee:** Data curation. **In-Woo Park:** Data curation. **Seung-Wook Ha:** Investigation. **Keyhong Park:** Resources, Data curation. **Hyun-Kwon Do:** Investigation. **Seong-Taek Yun:** Funding acquisition, Project administration, Writing - review & editing. **Kang-Kun Lee:** Funding acquisition, Supervision, Writing - review & editing.

Declaration of Competing Interest

The authors declare that there are no conflicts of interest.

Acknowledgements

This research was supported by a Korea Environmental Industry & Technology Institute (KEITI) grant entitled “R&D Project on Environmental Management of Geologic CO_2 Storage” (Project Number: 2018001810002), by a Korea Polar Research Institute grant (PE20140) and by a National Research Foundation of Korea (NRF) grant funded by the Korean government (MSIT) (NRF-2018R1C1B6007390). We thank all the members of the K-COSEM team and, appreciate Intae Kim and Minjung Kim for their efforts and support on noble gas analysis. Also, we appreciate the help of Dr. Stan E. Beaubien in interpreting the noble gas data. Finally, the authors would like to thank two anonymous reviewers for their detailed comments and observations which greatly improved the present paper.

Appendix A. Mass balance model

At least, two noble gases of different solubility are necessary to determine the degassed mass as outlined in Ju et al. (2019). The closed system is a one-step phase-partitioning process, and therefore, the degassed amount can be determined just by repeatedly adjusting the gas/liquid ratio until the result $((\frac{A}{B})_{(l)})$ fits into the measured data:

$$(\frac{A}{B})_{(g)} = (\frac{A}{B})_{(l)} \times \alpha$$

$$\alpha = \frac{\frac{r_A}{\phi_A} K_A}{\frac{r_B}{\phi_B} K_B}$$

Here:

$(\frac{A}{B})_{(g)}$ = A and B ratio in exsolved bubbles, where A and B are different noble gases

$(\frac{A}{B})_{(l)}$ = the composition of A and B remaining in the dissolved phase

α = partitioning coefficient for gas/liquid system

K_A, K_B = Henry's constant for A and B, from Sander et al., (2017)

r_A, r_B = dissolved-phase activity coefficients for A and B and

ϕ_A, ϕ_B = gas-phase fugacity coefficients for A and B.

In open system, the CO₂ bubble ($V_{(g)}$) is continuously lost into vadose zone carrying the noble gas tracers with it from the groundwater system until the plume is stabilized. An iteration calculation can be undertaken to account for the continuous loss and which terminates when the resultant mass ($m_{(l)}^i$) fits the observed noble gas data:

$$m_{A(l)}^i = m_{A(l)}^{i-1} - m_{A(g)}^{i-1}$$

$$m_{B(l)}^i = m_{B(l)}^{i-1} - m_{B(g)}^{i-1}$$

Here:

i = Iteration step

$m_{(l)}^{i-1}$ = mass in dissolved phase before $i - 1^{th}$ degassing loss (g)

$m_{(l)}^i$ = mass in dissolved phase after $i - 1^{th}$ degassing loss (g)

$m_{(g)}^{i-1}$ = degassed mass during $i - 1^{th}$ degassing process (g)

and degassed mass was determined from the degassed volume, such that:

$$m_{(g)}^{i-1} = C(V_{(g)} \times p^{i-1})$$

$$C = M/R \cdot T$$

$$p^{i-1} = \gamma K x^{i-1} / \phi$$

$$x^{i-1} = 18 [NG]^{i-1} (\rho_{(l)} V_{(l)})^{-1}$$

Here:

$V_{(g)}$ = degassed volume during $i - 1^{th}$ degassing process (cc)

C = conversion factor from volume to mass

M = molar mass (g/mol)

R = gas constant (8.314 cc·atm/K/mol)

T = temperature (K)

p^{i-1} = partial pressure of removed noble gas during $i - 1^{th}$ degassing process

K = Henry's constant in units of pressure (atm)

γ = liquid-phase activity coefficient

ϕ = gas-phase fugacity coefficient

x^{i-1} = molar fraction of noble gas in dissolved phase at $i - 1^{th}$ degassing moment ($mol_{NG}/mol_{(l)}$)

$[NG]^{i-1}$ = number of moles in dissolved phase at $i - 1^{th}$ degassing moment (mol)

$\rho_{(l)}$ = density of dissolved phase (g/cm³)

$V_{(l)}$ = volume of dissolved phase (cm³)

For an open system, an iterative model was used with a fixed $V_{(g)}$ value which should be small enough to finally achieve convergence with the measured noble gas composition. The noble gas concentration in the groundwater was gradually decreased in iterative steps. In the final stage ($i = n$), $\frac{m_{A(l)}^n}{m_{B(l)}^n}$ was matched against the monitored composition, and then the total degassed volume was calculated by multiplication of the bubble size ($V_{(g)}$) and the number of iteration steps (i) in the open system model.

Appendix B. Model optimization

Model optimization can be achieved in a similar manner to that used by Ballentine (1997) and Castro et al. (2009). The optimization aims to replicate the monitored noble gas data into a calculated mixing line with the smallest misfit to the observed data. As the monitored concentration is defined by mixing between two end-members, therefore, to achieve the minimum misfit, the end-members constituting the predicted mixing line were repeatedly updated. There are two end-members for the mixing line such as: 1) the noble gas concentration after the degassing event; and 2) the noble gas concentration of the background concentration (Supplementary Figure S3). The first end-member is the function of the initial amount and total degassed budget ($V_{(g)}$) of a species as discussed in the previous section. The second end-member is the function of excess air intrusion level (A)

to the Air Saturated Water (ASW) (Mazor and Bosch, 1987; Kipfer et al., 2002). Hence, this optimization process allows quantification of the degassing amount and the background level of leaked plume within the groundwater system. The optimization process is given by:

$$\chi^2 = \sum_{i=1}^N \left[\left(\frac{NG1_i^m - NG1_i^p}{\sigma_{NG1,i}} \right)^2 + \left(\frac{NG2_i^m - NG2_i^p}{\sigma_{NG2,i}} \right)^2 \right]$$

Here:

$i = i^{\text{th}}$ sample

N = the number of sample

σ = error of the observed data

$NG1^m$ = measured value of noble gas sample

$NG1^p$ = predicted value of noble gas sample from the arbitrary mixing line

This optimization process was conducted using a code compatible with the Matlab program.

Appendix C. Supplementary data

Supplementary material related to this article can be found, in the online version, at doi:<https://doi.org/10.1016/j.ijggc.2020.103041>.

References

- Alcalde, J., Flude, S., Wilkinson, M., Johnson, G., Edlmann, K., Bond, C.E., Scott, V., Gilfillan, S.M.V., Ogaya, X., Haszeldine, R.S., 2018. Estimating geological CO₂ storage security to deliver on climate mitigation. *Nat. Commun.* 9 (1), 2201. <https://doi.org/10.1038/s41467-018-04423-1>.
- Ballentine, C.J., 1997. Resolving the mantle He/Ne and crustal ²¹Ne/²²Ne in well gases. *Earth Planet. Sci. Lett.* 152 (1–4), 233–249. [https://doi.org/10.1016/S0012-821X\(97\)00142-8](https://doi.org/10.1016/S0012-821X(97)00142-8).
- Ballentine, C.J., O'Nions, R.K., Oxburgh, E.R., Horvath, F., Deak, J., 1991. Rare gas constraints on hydrocarbon accumulation, crustal degassing and groundwater flow in the Pannonian basin. *Earth Planet. Sci. Lett.* 105 (1–3), 229–246. [https://doi.org/10.1016/0012-821X\(91\)90133-3](https://doi.org/10.1016/0012-821X(91)90133-3).
- Ballentine, C.J., Schoell, M., Coleman, D., Cain, B.A., 2001. 300-Myr-old magmatic CO₂ in natural gas reservoirs of the west Texas Permian basin. *Nature* 409 (6818), 327. <https://doi.org/10.1038/35053046>.
- Ballentine, C.J., Burgess, R., Marty, B., 2002. Tracing fluid origin, transport and interaction in the crust. *Rev. Mineral. Geochem.* 47 (1), 539–614.
- Beaubien, S.E., Jones, D.G., Gal, F., Barkwith, A.K.A.P., Braibant, G., Baubron, J.C., Ciotoli, G., Graziani, S., Lister, T.R., Lombardi, S., Michel, K., Quattrocchi, F., Michel, K., 2013. Monitoring of near-surface gas geochemistry at the Weyburn, Canada, CO₂-EOR site, 2001–2011. *Int. J. Greenh. Gas Control* 16, 236–262. <https://doi.org/10.1016/j.ijggc.2013.01.013>.
- Beaubien, S.E., Bigi, S., Lombardi, S., Sacco, P., Tartarello, M.C., 2014. Groundwater changes caused by flow through naturally occurring gas (± water) leakage points. In: 4th EAGE CO₂ Geological Storage Workshop 2014. Stavanger; Norway. April 22–24, 2014.
- Brennwald, M.S., Kipfer, R., Imboden, D.M., 2005. Release of gas bubbles from lake sediment traced by noble gas isotopes in the sediment pore water. *Earth Planet. Sci. Lett.* 235 (1–2), 31–44. <https://doi.org/10.1016/j.epsl.2005.03.004>.
- Castro, M.C., Ma, L., Hall, C.M., 2009. A primordial, solar He–Ne signature in crustal fluids of a stable continental region. *Earth Planet. Sci. Lett.* 279 (3–4), 174–184. <https://doi.org/10.1016/j.epsl.2008.12.042>.
- Cohen, G., Loisy, C., Laveuf, C., Le Roux, O., Delaplace, P., Magnier, C., Rouchon, V., Garcia, B., Cerepi, A., 2013. The CO₂-Vadose project: experimental study and modelling of CO₂ induced leakage and tracers associated in the carbonate vadose zone. *Int. J. Greenh. Gas Control* 14, 128–140. <https://doi.org/10.1016/j.ijggc.2013.01.008>.
- Flude, S., Johnson, G., Gilfillan, S.M., Haszeldine, R.S., 2016. Inherent tracers for carbon capture and storage in sedimentary formations: composition and applications. *Environ. Sci. Technol.* 50 (15), 7939–7955. <https://doi.org/10.1021/acs.est.6b01548>.
- Flude, S., Györe, D., Stuart, F.M., Zurakowska, M., Boyce, A.J., Haszeldine, R.S., Chalaturnyk, R., Gilfillan, S.M.V., 2017. The inherent tracer fingerprint of captured CO₂. *Int. J. Greenh. Gas Control* 65, 40–54. <https://doi.org/10.1016/j.ijggc.2017.08.010>.
- Gilfillan, S.M.V., Ballentine, C.J., Holland, G., Blagburn, D., Sherwood Lollar, B., Scott, S., Schoell, M., Cassidy, M., 2008. The noble gas geochemistry of natural CO₂ gas reservoirs from the Colorado Plateau and Rocky Mountain provinces, USA. *Geochim. Cosmochim. Acta* 72, 1174–1198. <https://doi.org/10.1016/j.gca.2007.10.009>.
- Gilfillan, S.M.V., Lollar, B.S., Holland, G., Blagburn, D., Stevens, S., Schoell, M., Cassidy, M., Ding, Z., Zhou, Z., Lacrampe-Couloume, G., Ballentine, C.J., 2009. Solubility trapping in formation water as dominant CO₂ sink in natural gas fields. *Nature* 458 (7238), 614. <https://doi.org/10.1016/j.gca.2007.10.009>.
- Gilfillan, S.M.V., Wilkinson, M., Haszeldine, R.S., Shipton, Z.K., Nelson, S.T., Poreda, R.J., 2011. He and Ne as tracers of natural CO₂ migration up a fault from a deep reservoir. *Int. J. Greenh. Gas Control* 5 (6), 1507–1516. <https://doi.org/10.1016/j.ijggc.2011.08.008>.
- Gilfillan, S.M.V., Haszeldine, S., Stuart, F., Gyore, D., Kilgallon, R., Wilkinson, M., 2014. The application of noble gases and carbon stable isotopes in tracing the fate, migration and storage of CO₂. *Energy Procedia* 63, 4123–4133. <https://doi.org/10.1016/j.egypro.2014.11.443>.
- Gilfillan, S.M.V., Sherk, G.W., Poreda, R.J., Haszeldine, R.S., 2017. Using noble gas fingerprints at the Kerr Farm to assess CO₂ leakage allegations linked to the Weyburn-Midale CO₂ monitoring and storage project. *Int. J. Greenh. Gas Control* 63, 215–225. <https://doi.org/10.1016/j.ijggc.2017.05.015>.
- Harvey, O.R., Qafoku, N.P., Cantrell, K.J., Lee, G., Amonette, J.E., Brown, C.F., 2012. Geochemical implications of gas leakage associated with geologic CO₂ storage. *Crit. Rev. Environ. Sci. Technol.* 47 (1), 23–36. <https://doi.org/10.1021/es3029457>.
- Holland, G., Gilfillan, S., 2013. Application of noble gases to the viability of CO₂ storage. In: Burnard, P. (Ed.), *The Noble Gases as Geochemical Tracers. Advances in Isotope Geochemistry*. Springer, Berlin, Heidelberg, pp. 177–223. https://doi.org/10.1007/978-3-642-28836-4_8.
- Ide, S.T., Friedmann, S.J., Herzog, H.J., 2006. CO₂ leakage through existing wells: current technology and regulations. In 8th International Conference on Greenhouse Gas Control Technologies 19–22.
- IEAGHG, 2011. Potential Impacts on Groundwater Resources of CO₂ Storage. IEAGHG, Cheltenham, UK.
- IPCC, 2005. Intergovernmental Panel on Climate Change. Special Report on CO₂ Capture and Storage, Edited. pp. 208–210.
- Ju, Y., Kaown, D., Lee, K.K., 2018a. A three-pronged approach for identifying source and extent of nitrate contamination in groundwater. *J. Soil Water Conserv.* 73 (5), 493–503. <https://doi.org/10.2489/jswc.73.5.493>.
- Ju, Y., Lee, S.S., Kaown, D., Lee, K.K., 2018b. Application of inert gas tracers to identify the physical processes governing the mass balance problem of leaking CO₂ in shallow groundwater system. 14th Greenhouse Gas Control Technologies Conference; Melbourne; Australia; October 21–26. https://papers.ssrn.com/sol3/papers.cfm?abstract_id=3365686.
- Ju, Y., Beaubien, S.E., Lee, S.S., Kaown, D., Hahm, D., Lee, S., Park, I.W., Park, K., Yun, S.T., Lee, K.K., 2019. Application of natural and artificial tracers to constrain CO₂ leakage and degassing in the K-COSEM site, South Korea. *Int. J. of Greenh. Gas Control* 86, 211–225. <https://doi.org/10.1016/j.ijggc.2019.05.002>.
- Kilgallon, R., Gilfillan, S.M.V., Edlmann, K., McDermott, C.L., Naylor, M., Haszeldine, R.S., 2018. Experimental determination of noble gases and SF₆ as tracers of CO₂ flow through porous sandstone. *Chem. Geol.* 480, 93–104. <https://doi.org/10.1016/j.chemgeo.2017.09.022>.
- Kim, I., Hahm, D., Rhee, T.S., Kim, T.W., Kim, C.S., Lee, S., 2016. The distribution of glacial meltwater in the Amundsen Sea, Antarctica, revealed by dissolved helium and neon. *J. Geophys. Res. Oceans* 121 (3), 1654–1666. <https://doi.org/10.1002/2015JC011211>.
- Kipfer, R., Aeschbach-Hertig, W., Peeters, F., Stute, M., 2002. Noble gases in lakes and ground waters. *Rev. Mineral. Geochem.* 47 (1), 615–700. <https://doi.org/10.2138/rmg.2002.47.14>.
- LaForce, T., Ennis-King, J., Boreham, C., Paterson, L., 2014. Residual CO₂ saturation estimate using noble gas tracers in a single-well field test: the CO₂CRC Otway project. *Int. J. Greenh. Gas Control* 26, 9–21. <https://doi.org/10.1016/j.ijggc.2014.04.009>.
- Lee, K.K., Lee, S.H., Yun, S.T., Jeon, S.W., 2016. Shallow groundwater system monitoring on controlled CO₂ release sites: a review on field experimental methods and efforts for CO₂ leakage detection. *Geosci. J.* 20 (4), 569–583. <https://doi.org/10.1007/s12303-015-0060-z>.
- Lee, S.S., Kim, H.H., Joun, W.T., Lee, K.K., 2017. Design and construction of groundwater monitoring network at shallow-depth CO₂ injection and leak test site, Korea. *Energy Procedia* 114, 3060–3069. <https://doi.org/10.1016/j.egypro.2017.03.1434>.
- Lee, S.S., Ju, Y., Ha, S.W., Joun, W.T., Jun, S.C., Yun, S.T., Lee, K.K., 2018. Controlled CO₂ injection into a shallow aquifer and leakage detection monitoring by two different leakage events at the K-Cosem site, Korea. In 14th Greenhouse Gas Control Technologies Conference Melbourne; Australia; October 21–26. https://papers.ssrn.com/sol3/papers.cfm?abstract_id=3366360.
- Lemieux, J.M., 2011. The potential impact of underground geological storage of carbon dioxide in deep saline aquifers on shallow groundwater resources. *Hydrogeol. J.* 19

- (4), 757–778. <https://doi.org/10.1007/s10040-011-0715-4>.
- Lions, J., Devau, N., De Lary, L., Dupraz, S., Parmentier, M., Gombert, P., Dictor, M.C., 2014. Potential impacts of leakage from CO₂ geological storage on geochemical processes controlling fresh groundwater quality: a review. *Int. J. Greenh. Gas Control* 22, 165–175. <https://doi.org/10.1016/j.ijggc.2013.12.019>.
- Lollar, B.S., Ballentine, C.J., Onions, R.K., 1997. The fate of mantle-derived carbon in a continental sedimentary basin: integration of C/He relationships and stable isotope signatures. *Geochim. Cosmochim. Acta* 61 (11), 2295–2307. [https://doi.org/10.1016/S0016-7037\(97\)00083-5](https://doi.org/10.1016/S0016-7037(97)00083-5).
- Lott, D.E., Jenkins, W.J., 1998. Advances in analysis and shipboard processing of tritium and helium samples. *Int. WOCE Newsl.* 30, 27–30.
- Lu, J., Cook, P.J., Hosseini, S.A., Yang, C., Romanak, K.D., Zhang, T., Freifeld, B.M., Smyth, R.C., Zeng, H., Hovorka, S.D., 2012. Complex fluid flow revealed by monitoring CO₂ injection in a fluvial formation. *J. Geophys. Res. Solid Earth* 117. <https://doi.org/10.1029/2011JB008939>.
- Ma, L., Castro, M.C., Hall, C.M., 2009. Atmospheric noble gas signatures in deep Michigan Basin brines as indicators of a past thermal event. *Earth Planet. Sci. Lett.* 277 (1–2), 137–147. <https://doi.org/10.1016/j.epsl.2008.10.015>.
- Mackintosh, S.J., Ballentine, C.J., 2012. Using ³He/⁴He isotope ratios to identify the source of deep reservoir contributions to shallow fluids and soil gas. *Chem. Geol.* 304–305, 142–150. <https://doi.org/10.1016/j.chemgeo.2012.02.006>.
- Mazor, E., Bosch, A., 1987. Noble gases in formation fluids from deep sedimentary basins: a review. *Appl. Geochem.* 2 (5–6), 621–627. [https://doi.org/10.1016/0883-2927\(87\)90014-X](https://doi.org/10.1016/0883-2927(87)90014-X).
- Myers, M., Stalker, L., Pejic, B., Ross, A., 2013. Tracers—Past, present and future applications in CO₂ geosequestration. *Appl. Geochem.* 30, 125–135. <https://doi.org/10.1016/j.apgeochem.2012.06.001>.
- Nimz, G.J., Hudson, G.B., 2005. The use of noble gas isotopes for monitoring leakage of geologically stored CO₂. In: Thomas, D., Benson, S. (Eds.), *Carbon Dioxide Capture for Storage in Deep Geologic Formations*, vol. 2. Elsevier Press, Amsterdam, pp. 1113–1130.
- Parkhurst, D.L., Appelo, C.A.J., 2013. Description of input and examples for PHREEQC version 3: a computer program for speciation, batch-reaction, one-dimensional transport, and inverse geochemical calculations (No. 6-A43). US Geol. Survey. <https://doi.org/10.3133/tm6A43>.
- Pinti, D.L., Marty, B., 1995. Noble gases in crude oils from the Paris Basin, France: implications for the origin of fluids and constraints on oil-water-gas interactions. *Geochim. Cosmochim. Acta* 59 (16), 3389–3404. [https://doi.org/10.1016/0016-7037\(95\)00213-J](https://doi.org/10.1016/0016-7037(95)00213-J).
- Rillard, J., Loisy, C., Le Roux, O., Cerepi, A., Garcia, B., Noirez, S., Rouchon, V., Delaplace, P., Willequet, O., Bertrand, C., 2015. The DEMO-CO₂ project: a vadose zone CO₂ and tracer leakage field experiment. *Int. J. Greenh. Gas Control* 39, 302–317. <https://doi.org/10.1016/j.ijggc.2015.04.012>.
- Risk, D., Lavoie, M., Nickerson, N., 2015. Using the Kerr investigations at Weyburn to screen geochemical tracers for near-surface detection and attribution of leakage at CCS/EOR sites. *Int. J. Greenh. Gas Control* 35, 13–17. <https://doi.org/10.1016/j.ijggc.2015.01.019>.
- Sander, R., 2017. Henry's law constants. In: Linstrom, P.J., Mallard, W.G. (Eds.), *NIST Chemistry WebBook, NIST Standard Reference Database Number 69*. National Institute of Standards and Technology, Gaithersburg MD, pp. 20899. <https://doi.org/10.18434/T4D303>.
- Sathaye, K.J., Larson, T.E., Hesse, M.A., 2016. Noble gas fractionation during subsurface gas migration. *Earth Planet. Sci. Lett.* 450, 1–9. <https://doi.org/10.1016/j.epsl.2016.05.034>.
- Sechriest, R.E., 1960. Relationship between total alkalinity, conductivity, original pH, and buffer action of natural water. *Ohio J. Sci.* 60 (5), 303.
- Stalker, L., Boreham, C., Underschultz, J., Freifeld, B., Perkins, E., Schacht, U., Sharma, S., 2009. Geochemical monitoring at the CO₂CRC Otway Project: tracer injection and reservoir fluid acquisition. *Energy Procedia* 1 (1), 2119–2125. <https://doi.org/10.1016/j.egypro.2009.01.276>.
- Stalker, L., Boreham, C., Underschultz, J., Freifeld, B., Perkins, E., Schacht, U., Sharma, S., 2015. Application of tracers to measure, monitor and verify breakthrough of sequestered CO₂ at the CO₂CRC Otway Project, Victoria, Australia. *Chem. Geol.* 399, 2–19. <https://doi.org/10.1016/j.chemgeo.2014.12.006>.
- Stanley, R.H., Jenkins, W.J., Lott, D.E., Doney, S.C., 2009. Noble gas constraints on air-sea gas exchange and bubble fluxes. *J. Geophys. Res. Oceans* 114 (C11). <https://doi.org/10.1029/2009JC005396>.
- Vialle, S., Contraires, S., Zinzner, B., Clavaud, J.B., Mahiouz, K., Zuddas, P., Zamora, M., 2014. Percolation of CO₂-rich fluids in a limestone sample: evolution of hydraulic, electrical, chemical, and structural properties. *J. Geophys. Res. Solid Earth* 119 (4), 2828–2847. <https://doi.org/10.1002/2013JB010656>.
- Zheng, C., Bennett, G.D., 2002. *Applied Contaminant Transport Modeling*. Wiley-Interscience, New York.
- Zhou, Z., Ballentine, C.J., Kipfer, R., Schoell, M., Thibodeaux, S., 2005. Noble gas tracing of groundwater/coalbed methane interaction in the San Juan Basin, USA. *Geochim. Cosmochim. Acta* 69 (23), 5413–5428. <https://doi.org/10.1016/j.gca.2005.06.027>.